The Astrophysical Journal, 699:732–741, 2009 July 1 doi:10.1088/0004-637X/699/1/732

THE UNUSUAL SPECTRAL ENERGY DISTRIBUTION OF LBQS 0102–2713

Th. Boller[1], K. Linguri[2], T. Heftrich[3], and M. Weigand[3]
[1] Max-Planck-Institut für Extraterrestrische Physik, Garching, Germany; bol@mpe.mpg.de
[2] Secondary School, Neu-Isenburg, Germany
[3] Johann Wolfgang Goethe-University, Frankfurt am Main, Germany
Received 2008 December 16; accepted 2009 April 30; published 2009 June 15

ABSTRACT

We have studied the spectral energy distribution of the quasar LBQS 0102–2713. The available multiwavelength data in the observers frame are one optical spectrum between 3200 and 7400 Å, seven *Hubble Space Telescope* (*HST*) Faint Object Spectrograph (FOS) spectra between 1700 and 2300 Å, one *GALEX* NUV flux density and a K_S magnitude obtained from NASA/IPAC Extragalactic Database, and three public *ROSAT* PSPC pointed observations in the 0.1–2.4 keV energy band. The α_{ox} values obtained from the *HST* FOS, the optical spectrum, and the *ROSAT* observations are −2.3 and −2.2, respectively, comparable to broad absorption line (BAL) quasars. The 2500 Å luminosity density is about a factor of 10 higher compared to the mean of the most luminous Sloan Digital Sky Survey quasars. The 2 keV νL_ν value is lower by about a factor of 10 compared to the radio-loud quasars shown in Figure 10 of Richards et al. LBQS 0102–2713 exhibits one of the steepest soft X-ray photon indices obtained so far. For a simple power-law fit with leaving the N_H free in the fit, we obtain a photon index of $\Gamma = 6.0 \pm 1.3$. Fixing the N_H value to the Galactic value, the photon index still remains steep with a value of about 3.5. We argue that LBQS 0102–2713 is similar to BAL quasars with respect to their UV brightness and 2 keV X-ray weakness. However, the absorption by neutral matter is significantly lower compared to BAL quasars. The X-ray weakness is most probably not due intrinsically X-ray weakness based on the UV line strengths which are comparable to the line strength values reported in quasar composites. If the X-ray weakness will be confirmed in future observations, LBQS 0102–2713 might be indicative for a new class of quasars with an unusual combination in their UV, X-ray, and N_H properties.

Key words: galaxies: nuclei – galaxies: photometry – quasars: individual (LBQS 0102–2713)

Online-only material: color figures

1. INTRODUCTION

We report on the extreme-ultraviolet-to-X-ray spectral energy distribution (SED) of the quasar LBQS 0102–2713 using the spectral index α_{ox}. The α_{ox} value is defined as $\alpha_{ox} = 0.384 \times \log(L_{2\,keV})/(L_{2500\,Å})$. The α_{ox} value relates the relative efficiencies of emitted ultraviolet disk photons to the hard X-ray photons. This value is therefore an important tool to provide quantitative and qualitative constrains on models of the physical association between the UV and X-ray emission. The α_{ox} value obtained from the *Hubble Space Telescope* (*HST*) Faint Object Spectrograph (FOS) spectra (York 1990), the optical spectrum (Morris et al. 1991), and the *ROSAT* data are −2.3 or −2.2, respectively. The α_{ox} values are similar compared to broad absorption line (BAL) quasars (e.g., Gallagher et al. 2006). The authors have analyzed 35 BAL quasars based on *Chandra* observations. Their α_{ox} values range between −1.65 and −2.48. The majority of the objects have values smaller than −2.0. It is argued that the X-ray weakness of BAL quasars is due to neutral intrinsic absorption with column densities between about $(0.1–10) \times 10^{23}$ cm^{-2}. As more soft X-ray photons are expected for a simple neutral absorber, the absorption is assumed to be more complex. Partial covering or ionized absorbers can account for this observational fact.

Gibson et al. (2008) have analyzed *Chandra* and *XMM-Newton* observations of 536 Sloan Digital Sky Survey (SDSS) quasars. They find that radio-quiet BAL quasars tend to have steeper α_{ox} values compared to non-BAL quasars (their Figure 3). They constrain the fraction of X-ray weak non-BAL quasars and find that such objects are rare. Leighly et al. (2007) report on an α_{ox} value of −2.3 in the quasar PHL 1811. Miniutti et al. (2009) found values between −1.5 and −4.3 in PHL 1092. Similar results have been obtained by Strateva et al. (2005), Vignali et al. (2003), and Green et al. (2008). However, most of the objects with α_{ox} values close to −2 are upper limits. The dependence on α_{ox} as a function of redshift and the rest-frame ultraviolet luminosity has been investigated by Vignali et al. (2003), Strateva et al. (2005), and Green et al. (2008).

We also concentrate on the SED in the soft (0.1–2.4 keV) X-ray band based on *ROSAT* PSPC observations. We find that LBQS 0102–2713 might have an extreme value of the photon index of $\Gamma = (6.0 \pm 1.3)$. X-ray observations have shown Narrow-Line Seyfert 1 Galaxies (NLS1s) to have steep soft X-ray spectra as a class, first reported by Puchnarewicz et al. (1992). A significant correlation between the slope of the 0.1–2.4 keV X-ray continua and the FWHM of the Hβ line was found for Seyfert 1 galaxies (Boller et al. 1996). The distribution of the values Γ and FWHM Hβ show a continuous increase in the slope of the spectral continuum distribution with decreasing FWHM Hβ line width. This suggests that narrow- and broad-line Seyfert 1 galaxies form essentially the same class of objects and that there might be an underlying physical parameter which controls the distribution of objects. Smaller black hole masses could account for narrow Hβ line widths which require that NLS1 have to be accreting at higher fractions of their Eddington rates to maintain their relatively normal observed luminosities (Boller et al. 1996). *XMM-Newton* observations of IRAS 13224-3809 (Boller et al. 2003) and 1H 0707-495 (Boller et al. (2002) have confirmed that a shifted accretion disk spectrum accounts for the steep *ROSAT* photon indices. Steep soft photon indices have also been reported by other authors (e.g., Boller et al. 2000). Walter & Fink (1993) found values ranging between

1.5 and 3.4. Fiore et al. (1998) have used ASCA data on the quasars NAB 0205+024 and PG 1244+026 and found photon indices of $\Gamma = (3.22 \pm 0.24)$ and (2.95 ± 0.28), respectively. George et al. (2000) report on a photon index of $4.18^{0.82}_{1.1}$ in PG 0003+199. Grupe et al. (1995) identified in the *ROSAT* All-Sky Survey the ultrasoft AGN WPVS 007. The corresponding photon index is 8.3. Similarly to the correlation found in the soft energy range, a correlation between the slope of the 2–10 keV photon index, obtained from power-law fits to ASCA observations of broad- and narrow-line Seyfert 1 galaxies, and the width of the FWHM Hβ line, has been discovered by Brandt et al. (1997). Steep 2–10 keV X-ray continua, with values of the photon index between 1.9 and 2.6, are characteristic of NLS1s. One possible explanation suggested is that NLS1s may exhibit a cooler accretion disk corona (Pounds et al. 1995). A more detailed description of our knowledge on NLS1s is given by Trümper & Hasinger (2008).

The multiwavelength SED of radio-loud quasars has been investigated by Richards et al. (2006), building upon the quasar SED published by Elvis et al. (1994) for radio-quiet quasars. Richards et al. (2006) use mid-infrared data based on the *Spitzer Space Telescope*, SDSS photometry as well as near-infrared, *GALEX, VLA*, and *ROSAT* data. One of the most important results is the quasar SED shown in their Figure 10. The mean radio-quiet α_{ox} value from Elvis et al. (1994) is -1.5, while for radio-loud objects the mean value is -1.8 (Richards et al. 2006).

LBQS 0102–2713 is a quasar at a redshift of 0.78. The object was selected from the *ROSAT* PSPC catalog via the hardness ratio 1 (HR1)[4] criteria in the range from -0.5 to -0.7 derived from a reference sample of known steep spectrum active galactic nuclei (AGNs). LBQS 0102–2713 showed the steepest photon index from the selected sample. Here we concentrate on three public *ROSAT* PSPC observations, an optical spectrum between 3200 and 7400 Å observed in 1988 (Morris et al. 1991), seven *HST* FOS spectra between 1700 and 2300 Å, and one *GALEX* NUV flux density available at NED. High-energy data above 2.4 keV are not available presently. In Section 2, we describe the X-ray observations and data analysis. The results from the X-ray fitting analysis are given in Section 3. Section 4 contains the results from the α_{ox} analysis. The comparison with mean SEDs is given in Section 5. Models for the X-ray weakness are presented in Section 6. Section 7 contains the summary and open problems. In Section 8, we list security checks on the identification of LBQS 0102–2713 as an X-ray source. Throughout the paper, we adopt $H_0 = 70$ km s^{-1} and a Λ-cosmology of $\Omega_M = 0.3$ and $\Omega_\Lambda = 0.7$.

2. X-RAY OBSERVATIONS AND DATA ANALYSIS

The object was observed three times with the *ROSAT* PSPC detector in 1992 (compared to Table 1 for the observation log file). The source is located off-axis in the PSPC detector with a separation from the pointing direction of about $0.^{\circ}5$. The data were retrieved from the MPE archive. The PSPC data in the MPE archive were processed at MPE and copied to HEASARC. The *ROSAT* data in both archives are identical.

The *ROSAT* data were converted into FITS files using the *xselect* command-line interface version 2.4. The observations were converted into FITS files and a merged FITS file was created from the two longer observations (ROR numbers 700121p-0 and 700121p-2). The short observation (ROR number 700121p-1) is highly background dominated and the source is not significantly detected. Therefore, the results from the spectral fitting are only presented for the two long observations and the corresponding merged data set. The *xselect* command-line interfaces handles RDF FITS format files. In the RDF case, the events are for instance in the file rp700121a00_bas.fits file (the basic file) for ROR number 700121p-0. Using the *read events* command the two single observations and the merged observation the were read into *xselect*. *ROSAT* images were created via *extract image* and *saoimage*. For all three observations used for subsequent spectral fitting, the source region was extracted at R.A. = $01^{h}04^{m}40.^{s}9$ and decl. = $-26^{o}57^{m}07^{s}$. The background region was extracted at R.A. = $01^{h}04^{m}09^{s}$ and decl. = $-26^{o}45^{m}04^{s}$. The source and background extraction radii are 320 arcsec. Finally, using *extract spectrum* and *save spectrum* the source and background fits files were created. The corresponding *ROSAT* response matrix is *pspcb_92mar11.rsp*.

Table 1
Observation Log Data of the *ROSAT* PSPC Observations of LBQS 0102–2713

ROR Number	Date	Observation Duration (s)
700121p-0	1992 Jan 5	6157
700121p-1	1992 Jun 5	2191
700121p-2	1992 Dec 8	6724

We have analyzed the *ROSAT* PSPC observations of LBQS 0102–2713 independently from the *xselect* command-line interface with the *EXSAS* software routines (Zimmermann et al. 1994) developed for analyzing *ROSAT* data based on the *MIDAS* software package for the two long observations 700121p-0 and 700121p-2. A merged data file was also created with the *EXSAS* command *intape/disk*. Energy channels were selected from 8 to 240 using the *EXSAS prepare-spectrum* programme.

3. SPECTRAL FITTING

In the *ROSAT* All-Sky Survey (RASS), we get 26 source counts with a mean exposure of 333 s. The extraction radius is 500 arcsec. For the background we get 16 counts with a mean exposure of 435 s and an extraction radius of 500 arcsec. This results in 10 net counts and a mean count rate of 0.02 counts s^{-1}. With these numbers no reliable fits could be obtained from the RASS data. For the merged data sets of the PSPC pointings, we get 1351 source counts and 741 background counts for a total exposure of 12881 s. This results in 610 net counts and a mean count rate of 0.05 counts s^{-1}. With these numbers and the limited spectral energy resolution of *ROSAT*, only a limited range of models can be fitted. We present the results only for a simple power-law fit with cold absorption and a disk blackbody model. Longer X-ray observation with the present generation of X-ray satellites are required to present more advanced model fits, e.g., a smeared absorption model according to Schurch & Done (2006), or a disk reflection model following Crummy et al. (2006).

3.1. xselect Command-Line Interface and EXSAS Spectral Power-Law Fitting

The source spectra obtained from the ROR numbers 700121p-0 and 700121p-2 using the *xselect* command-line interface were grouped with the *grppha* command with *group min 10*. The merged data set was grouped with *group min 30*. The

[4] The hardness ratio 1 is defined as HR1 = ((52 − 102) − (11 − 41))/((11 − 41) + (52 − 201)) (Zimmermann et al. 1994). The numbers refer to the *ROSAT* PSPC channels.

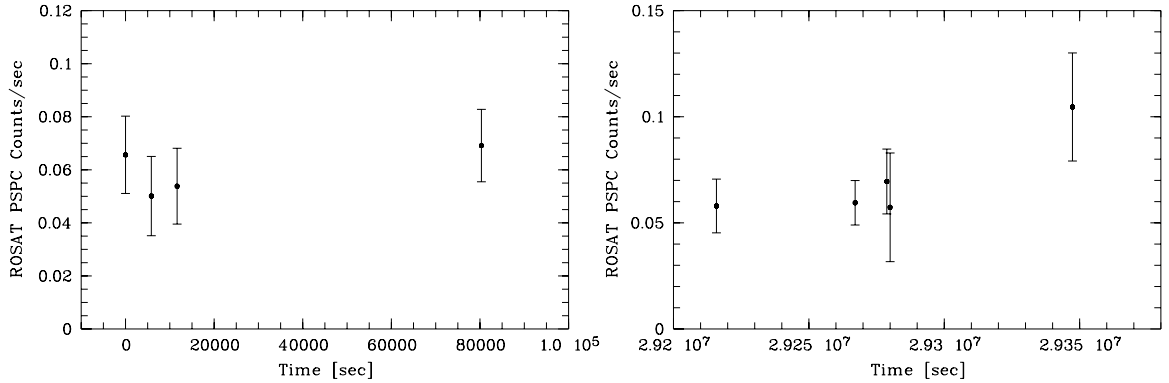

Figure 1. *ROSAT* PSPC light curves of LBQS 0102–2713 observed in 1992 January (left panel) and 1992 December (right panel). The bin size is 4000 s. The source shows no significant X-ray variability between the two observations.

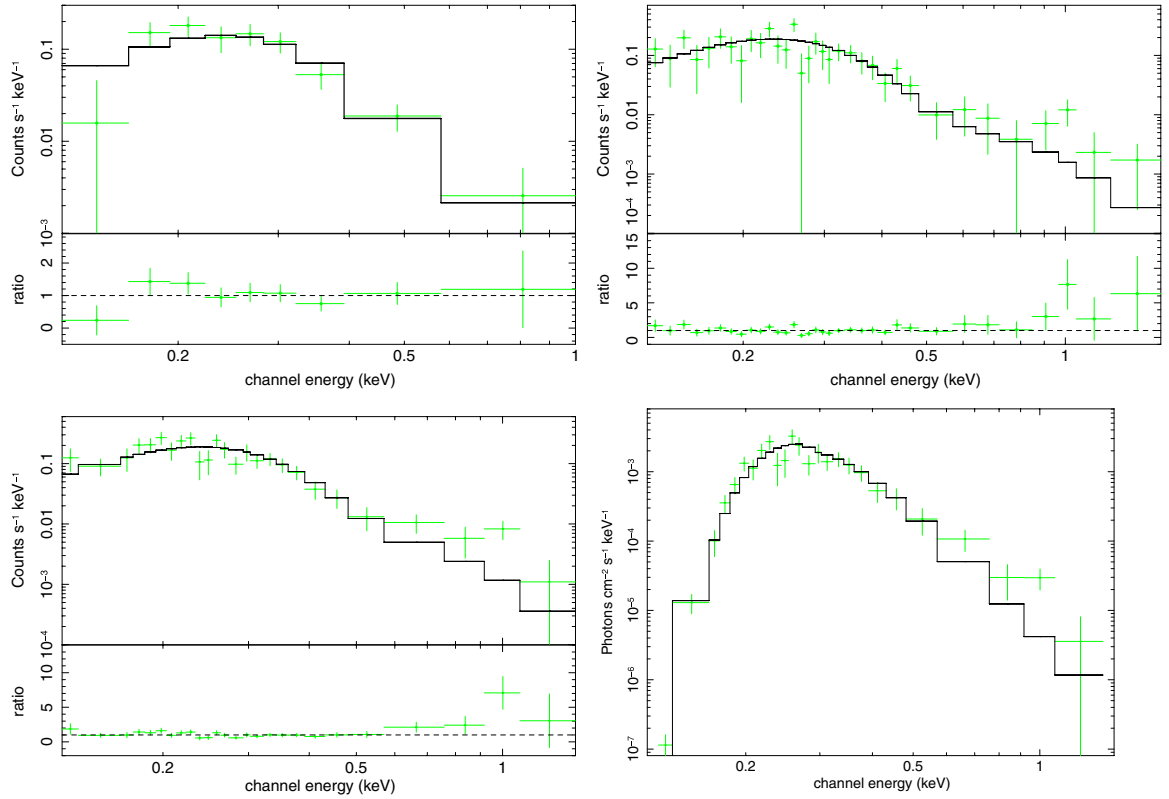

Figure 2. *ROSAT* PSPC observation of LBQS 0102–2713 from 1992 January and 1992 December (upper left and right panels). The lower left panel shows the fit to the merged data set. Applying a simple power-law fit and leaving the absorption parameter free, we obtain from the *xselect* analysis photon indices of 6.6 ± 2.5, 5.5 ± 2.5, and 6.0 ± 1.3, respectively. The unfolded spectrum obtained from the merged data set is shown in the lower right panel.

(A color version of this figure is available in the online journal.)

spectral fitting was performed using *XSPEC* version 12.5.0. The model components were (mo = phabs (zpo)). While the light curves do not show significant variations (Figure 1) the resulting photon indices are remarkably steep (Figure 2). LBQS 0102–2713 might be the quasar with the steepest soft X-ray photon index, detected in two individual and the merged observations, reported so far. For the merged data set we get $\Gamma = (6.0 \pm 1.3)$ and $\Gamma = (5.8 \pm 1.3)$ for the *xselect* and *EXSAS* software packages, respectively. The spectral fitting results from the *xselect* command line interface and the *EXSAS* software routines are listed in Table 2. The spectral parameters obtained from both software systems are consistent within the errors. As a security check we have used the NASA GSFC simulation software *webpimms*. The simulated spectra are consistent with the *ROSAT* power-law fits. This is an independent test, whether the calibration and response files available at the MPE site give the same results as the corresponding files produced by the NASA GSFC calibration team.

3.2. Γ–N_H Contour Plots

The Galactic foreground absorption in the direction to LBQS 0102–2713 is very low with $N_H = 1.2 \times 10^{20}\mathrm{cm}^{-2}$. It is known that Γ and N_H are correlated in *ROSAT* PSPC fits, such that a larger N_H requires a steeper photon index to give a good fit. In Figure 3 we show the Γ–N_H contour plots for the merged data set and for the ROR number 700121p-2. For the ROR number 700121p-0 no reliable contour plot could be obtained. At a 99% confidence level, the photon index is about 3.5 at the Galactic N_H value. The photon index might indeed be flatter as

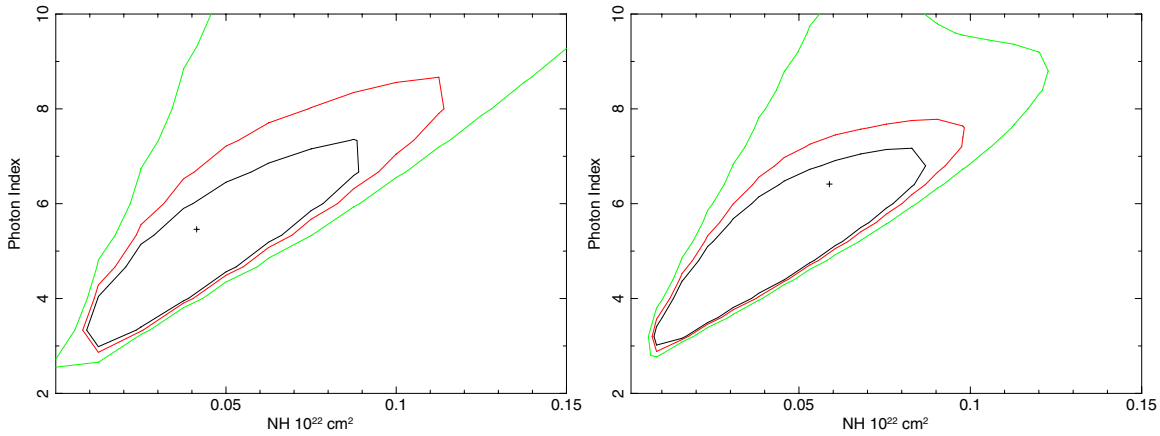

Figure 3. Γ–N_H contour plots obtained from ROR number 700121p-0 (left panel) and from the merged data set (right panel). The contour lines correspond to 68%, 90%, and 99% confidence levels. The low Galactic N_H value of 1.2×10^{20} cm^{-2} is within the 99% confidence level resulting in a photon index of about 3.5. The photon index might therefore be flatter as indicated by the power-law fits and LBQS 0102–2713 might be less special in X-rays.

(A color version of this figure is available in the online journal.)

Table 2
Spectral Fitting Results for a Power-Law Model with Foreground Absorption of LBQS 0102–2713[a]

ROR number	*xselect*			*EXSAS*		
	Γ	N_H	Norm	Γ	N_H	Norm
700121p-0	6.6 ± 2.5	6.2 ± 0.5	2.5 ± 2.9	5.5 ± 2.5	7.4 ± 1.5	4.2 ± 5.0
700121p-2	5.5 ± 2.5	3.7 ± 2.4	1.3 ± 1.8	6.5 ± 2.1	6.0 ± 4.7	4.5 ± 4.0
Merge data set	6.0 ± 1.3	4.8 ± 1.5	1.3 ± 1.6	5.8 ± 1.3	6.5 ± 4.4	1.5 ± 1.0

Note. [a] The N_H value is in units of 10^{20} cm^{-2} and the normalization is given in 10^{-4} photons cm^{-2} s^{-1} keV^{-1} at 1 keV.

$\Gamma = (6.0 \pm 1.3)$ and the object may be less special in X-rays than it appears from the simple power-law fits. However, the photon index obtained for a power-law fit with the Galactic N_H value fixed remains still steep for quasar soft X-ray SEDs (compared to Section 1). Longer observations with the present generation of X-ray telescopes are required to confirm whether the photon index of LBQS 0102–2713 is indeed extremely steep.

3.3. Ionized Absorber Plus Power-Law Spectral Modeling

We note that a simulation of a power law plus an ionized absorber could also result into a flatter photon index. A simulated 50 ks *XMM-Newton* spectrum obtained from a power-law model with cold absorption plus an ionized absorber based on the *grid25BIG_mt.fits* model (C. Done 2008, private communication) gives a photon index of $\Gamma = (4.4 \pm 0.5)$ for a column density of the ionized absorber ranging between $(1.1–1.5) \times 10^{22}$ cm^{-2} and an ionization parameter range between $\xi = 20$ and 30. The parameter ranges explored range between $N_H = 10^{21-24}$cm^{-2} and $\xi = 10$ to 1000. The flatter photon index occurs in a very narrow parameter range of the ionized absorber column density and the ionization value. When fitting the simulated data with the *ROSAT* PSPC response and the *ROSAT* exposure time, the photon index is (6.7 ± 1.8), consistent with the *ROSAT* spectral fitting results for a power-law model with the N_H value leaving free in the fit.

3.4. Blackbody Spectral Fitting Results

A blackbody fit to the merged data set does also result into an acceptable fit. The derived spectral parameters in the rest frame are: $N_H = (2.0 \pm 2.3) \times 10^{20}$cm^{-2}, $kT = (0.13 \pm 0.013)$ keV, and $n = (2.6 \pm 2.8) \times 10^{-5}$ photons cm^{-2} s^{-1} keV^{-1} at 1 keV. Due to the limited spectral resolution of *ROSAT*, we cannot disentangle between a power-law and a blackbody model. We compare the derived blackbody temperature with other published blackbody temperatures and find that they are in good agreement. Crummy et al. (2006) found values for the blackbody temperature for an AGN sample observed with *XMM-Newton* between 0.009 and 0.17 keV (their Table 2). Tanaka et al. (2005) have analyzed NLS1 spectra observed with *XMM-Newton* and found for a sample of 17 objects blackbody temperatures between 0.09 and 0.15 keV. Fiore et al. (1998) obtain blackbody temperatures of 0.16 keV for PG 1244+026 and NAB 0205+024, respectively based on ASCA observations. Puchnarewicz et al. (2001) obtain a value of 0.13 keV for the NLS1 galaxy RE J1034+396.

4. DERIVING THE α_{ox} VALUE FOR LBQS 0102–2713

4.1. Deriving the 2500 Å Flux Density from the Optical Spectrum

Morris et al. (1991) have published an optical spectrum of LBQS 0102–2713 in the wavelength range between 3200 and 7400 Å in the observers frame (compared to Figure 4). The Mg II line at 2800 Å (rest frame) is clearly visible. Applying a Gaussian fit to this line we obtain a FWHM value of about 2200 km s^{-1} in the rest frame. This value is very close to the artificial border line between NLS1 galaxies and broad line Seyfert galaxies of 2000 km s^{-1} following the definition of Osterbrock & Pogge (1985). In addition Morris et al. (1991) first noted the strong UV Fe II multiplet emission between about 2200 and 2500 Å in the rest frame. All this is typical for NLS1 galaxies and LBQS 0102–2713 can be considered as an X-ray bright NLS1 galaxy. This goes in line with the steep X-ray spectrum. In addition, a strong C III line is found at 1909 Å

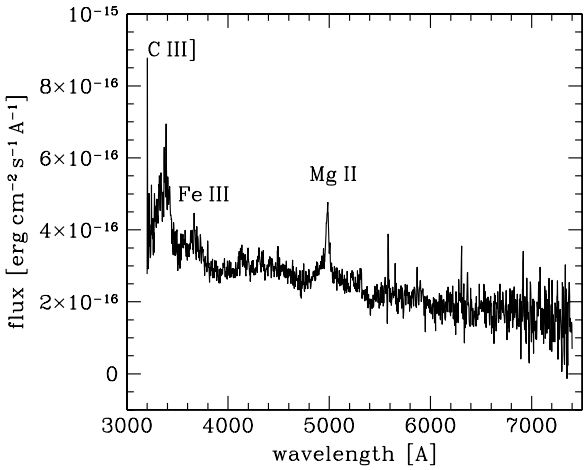

Figure 4. Optical spectrum of the quasar LBQS 0102–2713 obtained by Morris et al. (1991) obtained in 1988. The strongest emission lines of C III, Fe III, and Mg II are marked. Between the Fe III and the Mg II emission, there is a strong Fe II UV multiplet emission between about 2200 and 2500 Å rest-frame wavelength, first noted by Morris et al. (1991).

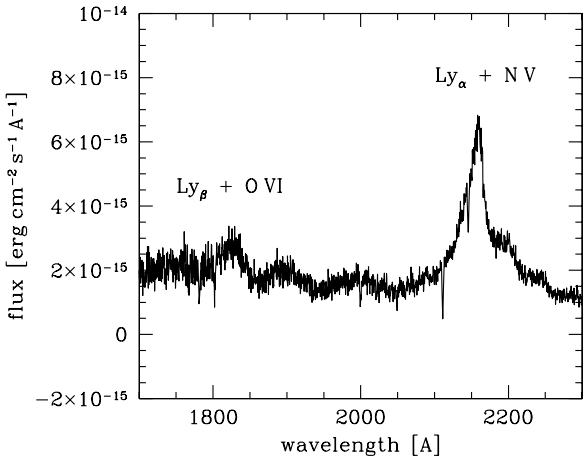

Figure 5. *HST* FOS spectra of the quasar LBQS 0102–2713 obtained from data set Y30901012T obtained in 1995. The strongest UV emission lines are marked and their EW values are comparable to those found in composite quasar spectra (compared to Section 6.1).

rest frame and a strong emission feature at about 2075 Å which is usually interpreted as a bunch of Fe III multiplets. The later feature is cataloged in the Vanden Berk et al. (2001) quasar composite paper and is certainly present in higher signal-to-noise composites.

The observed 4450 Å flux density from the optical spectrum (compared to Figure 4) obtained in 1988 is about $f^{\rm obs.}_{4450\ \text{Å}} = 3.0 \times 10^{-16}$ erg cm^{-2} s^{-1} Å^{-1}. Details of the spectroscopic measurements can be found in Section 2.3 of Morris et al. (1991). To convert the units from Å to Hz, we followed the relation from Hogg (2000) described in his Chapter 7. As the differential flux per unit log frequency or log wavelength is $\nu f_\nu = \lambda f_\lambda$ (Hogg uses S instead of f) one gets $f_\nu = (\lambda^2/c) \times f_\lambda$ with $f_\lambda = f^{\rm obs.}_{4450\ \text{Å}}$ and $\lambda = 4450$ Å. The resulting observed flux density per Hz is $f^{\rm obs.}_{4500\ \text{Å}} = 2.0 \times 10^{-27}$erg cm^{-2} s^{-1} Hz^{-1}. To correct the monochromatic flux measurements for Galactic extinction, we used the Nandy et al. (1975) extinction law with $R = A_V/E(B-V)$. Their Table 3 gives for $(1/\lambda(\mu\ \text{m}^{-1}))$ at 4450 Å an R value of 3.8. The $E(B-V)$ value from the *GALEX* data obtained from NED is 0.02. According to Geminale & Popowski (2005), the relation between R and ϵ is $\epsilon(\lambda - V) = R((A_\lambda/A_V) - 1)$. Following their extinction curves shown in Figure 4, one obtains an ϵ value of about 0.5. The A_λ value at 4450 Å is then 0.076 and the A_V value using the relations given above is 0.066. The A_λ/A_V value is 1.15. The extinction-corrected flux and the uncorrected flux at 4450 Å are related by $f^{\rm Ext.}_{4450\ \text{Å}} = (10^{+4} \times A_\lambda/A_V) \times f^{\rm obs.}_{4450\ \text{Å}} = 2.6 \times f^{\rm obs.}_{4450\ \text{Å}} = 5.3 \times 10^{-27}$erg cm^{-2} s^{-1} Hz^{-1}. The luminosity distance $D_L = 1.5 \times 10^{28}$cm. The resulting rest-frame UV luminosity density is $L_{2500\ \text{Å}} = 1.6 \times 10^{31}$ erg s^{-1} Hz^{-1}. The relation between $l_{\rm uv}$ and $L_{2500\ \text{Å}}$ is $\log L_{2500\ \text{Å}} = l_{\rm uv} = 31.21$.

4.2. Deriving the 2500 Å Flux Density from the HST FOS Spectra

We also analyzed the seven *HST* FOS spectra named as Y309010nT with n ranging from 2 to 8. The *HST* FOS spectra were obtained from the *HST* FOS proposal ID 6007: Comparison of the large scale structure in QSO absorbers and galaxies in the Galactic Poles, D. York, University of Chicago. The observed wavelength ranges between 1700 and 2300 Å. All seven exposures obtained in 1995 agree in their flux density values and the *HST* FOS absolute and relative calibration is very good (M. Rosa, ESO Garching 2009, private communication). In Figure 5, we show the spectrum for the science exposure number Y3090102T. The Lyα line is clearly visible and marked in the spectrum. The line is blended with a low-ionization line of N v at 1240 and 1242 Å in the rest frame. In addition, there is emission from the Lyβ line blended with the O VI line at 1032 and 1037 Å at their rest-frame wavelengths.

The observed 2300 Å flux density is about $f^{\rm obs.}_{2300\ \text{Å}} = 1.5 \times 10^{-15}$ erg cm^{-2} s^{-1} Å^{-1}. The flux density at 2500 Å rest frame is $f_{2500\ \text{Å}} = f_{1292\ \text{Å}} \times (1292\ \text{Å}/2500\ \text{Å})^{-0.5} = 4.2 \times 10^{-27}$ erg cm^{-2} s^{-1} Hz^{-1}. To extrapolate the corresponding rest-frame wavelength of 1292–2500 Å, we have used the $\alpha_{\rm o}$ value of -0.5 of Richstone & Schmidt (1980). The extinction-corrected flux at 2500 Å is 1.4×10^{-26} erg cm^{-2} s^{-1} Hz^{-1}, about a factor of 3.3 larger compared to the non-extinction-corrected flux density. The slight discrepancy compared to the optical spectrum obtained by Morris et al. (1991) might be due to flux variability between the 1988 and 1995 observations or due to the extrapolation from 1292 to 2500 Å using a mean $\alpha_{\rm o}$ value of -0.5. The correction for Galactic extinction has been performed as described in the previous subsection. The R value at 2500 Å is 7.2 and the ϵ value is 7.2. The resulting A_λ/A_V value is 1.4. This results into a Galactic extinction correction with a factor of 3.3 and the extinction-corrected flux is $f^{\rm Ext.}_{2500\ \text{Å}} = 1.4 \times 10^{-26}$ erg cm^{-2} s^{-1} Hz^{-1}. The resulting rest-frame luminosity density is $L_{2500\ \text{Å}} = 4.0 \times 10^{31}$ erg s^{-1} Hz^{-1}.

4.3. Deriving the 2 keV Flux Density from the Merged ROSAT PSPC Data Set

The 2 keV rest-frame flux density is determined following Hogg (2000) and Weedman's (1986) Quasar Astronomy (Section 3.5, page 61). The photon index Γ is related to the energy index via $\alpha_{\rm x} = -\Gamma + 1$. For a photon index not equal to 2, the rest-frame 2 keV flux density is given by $f_{2\ \text{keV}} = f(0.5\text{–}2.0) \times ((1+\alpha_x)/(1+z)^{\alpha_x})) \times ((\nu^{\alpha_x}_{2\ \text{keV}}/(\nu^{\alpha_x+1}_{2\ \text{keV}} - \nu^{\alpha_x+1}_{0.5\ \text{keV}}))$. The unabsorbed *ROSAT* flux in the 0.5–2.0 keV energy band is 4.3×10^{-14} erg cm^{-2} s^{-1}. As the photon index derived in the previous section was 6.0, we get for $\alpha_{\rm x}$ a value of -5. The corresponding 2 keV and

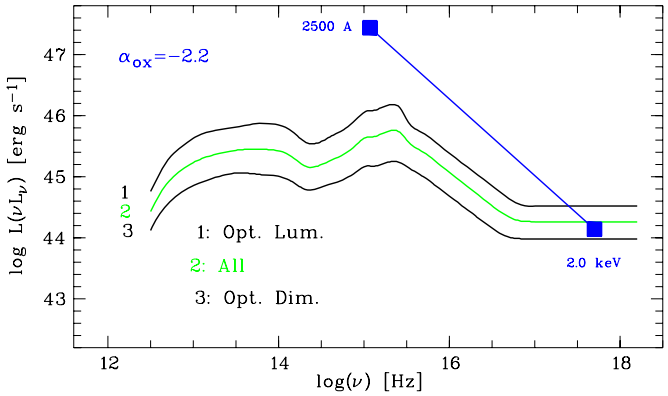

Figure 6. Comparison of the νL_ν values in the UV and in the X-rays with the mean SEDs for SDSS quasars. While the object is UV bright compared to the mean of the most luminous SDSS quasars (although there might be large scatter in the individual luminosities), the 2 keV value is comparable to the SDSS dim quasars.

(A color version of this figure is available in the online journal.)

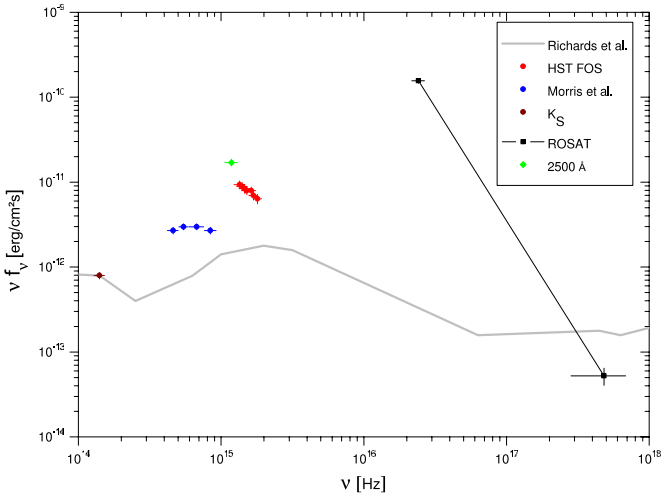

Figure 7. Optical spectrum from Morris et al. (1991), the *HST* FOS data, the *ROSAT* data, and the K_S value in the rest frame. The SED of LBQS 0102–2713 is normalized at the frequency of the K_S νf_ν value. The unnormalized νf_ν value and the normalized one are 5.6×10^{-13} erg cm^{-2} s^{-1} and 7.9×10^{-13} erg cm^{-2} s^{-1}, resulting into a normalization factor of 1.4. While in the UV the object is bright compared to the mean, at X-rays the object is X-ray weak. We find a strong discrepancy between the X-ray and the *HST* FOS UV data. The data obtained from the optical spectrum are most probably dominated by the host galaxy.

(A color version of this figure is available in the online journal.)

0.5 keV frequencies are 4.8×10^{17} Hz and 1.2×10^{17} Hz. This results into a flux density at 2 keV of $f_{\nu\,2\,\mathrm{keV}} = 4.3 \times 10^{-32}$ erg cm^{-2} s^{-1} Hz^{-1}. The 2 keV luminosity density is then $L_{2\,\mathrm{keV}} = 4.0 \times 10^{25}$ erg s^{-1} Hz^{-1}. We note that the extremely steep photon index has to be confirmed in future observations with the present generation of X-ray telescopes given the results from the contour plots shown in Figure 3. If the X-ray spectrum is flatter than obtained from the power-law fits, this would result in a less extreme α_{ox} value.

For a definition of $\alpha_{ox} = 0.384 \times \log(L_{2\,\mathrm{keV}}/L_{2500\,\text{Å}})$, one derives α_{ox} values of −2.3 and −2.2.

5. COMPARISON WITH QUASAR SEDS

5.1. Comparison with Mean SDSS Quasar SEDs

Richards et al. (2006) show the mean quasar SEDs for optically luminous SDSS, all SDSS, and optically dim quasars (compared to Figure 11 of their paper). In Figure 6, we show an adopted version of the plot of Richards et al. (2006). The νL_ν value at 2500 Å rest-frame wavelength is 4×10^{47} erg s^{-1}. This is about a factor of 10 more luminous compared to the mean of the optically most luminous SDSS quasars. However, there is a large dispersion in the optical M_B magnitudes for quasars. Brotherton et al. (2001) show the distribution of the M_B magnitudes for more than 11,000 quasars (their Figure 5). Their absolute magnitudes range between about -23^{mag} to -32^{mag}. LBQS 0102–2713 has a photometric IIIa-J magnitude of 17.52 mag as taken from NED at a wavelength of 4612 Å corresponding to 0.46 μm. This close to the mean B wavelength of 0.40 μm. The corresponding M_B value of LBQS 0102–2713 is −25.9. This might indicate that the scatter in the 2500 Å luminosities is also large and that LBQS 0102–2713 is less extreme in the UV than one would think at first glance when comparing the UV value to the mean of the optically most luminous quasars. The corresponding 2.0 keV rest-frame value of νL_ν value is 1.4×10^{44} erg s^{-1} which is comparable to the optically dim SDSS quasars. The dispersion in the X-rays appears to be much less compared to the UV luminosities if one compares the X-ray luminosity of LBQS 0102–2713 to the X-ray luminosities as shown in the sample papers of Strateva et al. (2005), Vignali et al. (2003), or Gibson et al. (2008).

5.2. Comparison with the Quasar SED for Radio-Loud Quasars

In Figure 7, we have plotted the available multiwavelength data in units of νf_ν versus the wavelength and compare these data points to the mean quasar SED for radio-loud objects from Richards et al. (2006, their Figure 10). All data points are extinction corrected. For the *ROSAT* data, we show only the lowest and highest energy data point. While at 2 keV the object is X-ray weak compared to the mean quasar SED, at the softest energies LBQS 0102–2713 is a very powerful emitter and the νf_ν value even exceeds the 2500 Å UV value. The *HST* FOS data points are about a factor of 2–5 larger compared to the mean quasar SED. Here we note again that the scatter in the individual UV luminosities compared to the mean might be larger as pointed out in the previous subsection and that therefore the object might be less extreme in its UV luminosity. The optical data points and the K_S magnitude follow the mean quasar SED. The main result from this plot is the discrepancy between the X-ray and *HST* FOS data points as these bands are discontinuous. The standard picture assumes that the rest-frame UV photons are emitted from the accretion disk and that the hard X-ray photons are arising from the accretion disk corona. From Figure 7, it is obvious that there is a discrepancy between the UV and the X-ray photons. The optical data from Morris et al. (1991) are also offset with respect to the *HST* FOS data points. This is most probably due to a significant contribution from the host galaxy and the rest-frame optical photons are not expected to be related to the accretion disk. We have cross-checked the discontinuity between the UV and X-ray data points. The *GALEX* NUV wavelength is 2315.7 Å (compared to Morrissey et al. 2007, their Table 1). The NUV *GALEX* calibrated flux from NED is 282.2 μJy. This converts into flux densities of 2.8×10^{-27} erg cm^{-2} s^{-1} Hz^{-1} or 1.6×10^{-15} erg cm^{-2} s^{-1} Å^{-1}. The *GALEX* NUV flux density value is consistent with the flux density shown in the *HST* FOS spectrum of Figure 5.

6. MODELS FOR THE X-RAY WEAKNESS

6.1. The Intrinsically Weakness Model

Leighly et al. (2007) favor an intrinsically X-ray weakness model for the quasar PHL 1811. The 2 keV X-ray emission is intrinsically weak rather than absorbed. In this case, one expects weak low ionization of semiforbidden UV lines. For the blend of the Lyα and N v lines, an EW value of 15 eV is obtained. No EW values are given for the blend of Lyβ and O VI. The authors argue that this points to an intrinsically weak X-ray model. The argumentation for an intrinsically X-ray weakness model is based on individual lines such as Na I D, Ca II H and K, and C IV. The rest-frame EW values for the blend of Lyβ and the O VI lines and the Lyα and the N v lines shown in Figure 5 are about 12 and 50 Å, respectively. In the following, we compare these values with quasar composite spectra. Brotherton et al. (2001) give for the Lyβ plus O VI lines an EW value of 11 Å in the rest frame. For the blend of Lyα and N v, the EW value is 87 Å. The corresponding values reported by Vanden Berk et al. (2001) are 9 and 94 Å, respectively. Zheng et al. (1997) found values of 16 and 102 Å, respectively. The EW values obtained for LBQS 0102–2713 are typical to the mean quasar composite values and the source appears not to be intrinsically X-ray weak.

6.2. Other Models

There are other models in the literature which are speculative or do have a low probability to explain the X-ray weakness.

Gibson et al. (2008) present in their Figure 2 a decreasing trend of α_{ox} with increasing 2500 Å UV luminosity density. This is a strong observational constraint as an increased UV luminosity density results into steeper α_{ox} values. In the case of PHL 1811 and LBQS 0102–2713, we indeed see lower 2 keV flux densities compared to other quasars. If one compares the UV and X-ray luminosity densities of LBQS 0102–2713 which are $\log l_{UV} = 31.20$ for the Morris et al. (1991) spectrum and $\log l_{UV} = 31.60$ obtained from the *HST* FOS spectra and an X-ray luminosity density of $\log l_X = 25.60$ obtained from *ROSAT*, with Figure 8 of Vignali et al. (2003) the X-ray weakness becomes immediately apparent. The reason for the so-called global X-ray Baldwin effect is presently not known. It is speculated that a patchy or disrupted accretion disk corona is related to the UV luminosity density (Gibson et al. 2008). However, there is no direct observational proof for this model.

One could speculate that UV and X-ray variability of the source might account for the low α_{ox} value. Assuming that LBQS 0102–2713 was in 1992 in a low X-ray flux state, then a factor of about 10 at 2 keV is required to obtain the canonical α_{ox} value of -1.8 for radio-loud quasar as shown in Figure 11 of Richards et al. (2006). A factor of 10 in three years with respect to the optical observations appears unlikely as only a few AGNs are known to exhibit flux variability of a factor of 10 or more. In addition, variability seems unlikely given Hook et al. (1994) who find only weak optical variability with $\sigma = 0.17$.

7. SUMMARY AND OPEN PROBLEMS

7.1. Comparison to BAL Quasars and a Possible Unique Combination of UV Brightness, X-ray Weakness, and Low N_H Values

LBQS 0102–2713 appears to be very similar to BAL quasars which show strong UV- and weak 2 keV X-ray emission (compared to Gallagher et al. 2006). Their α_{ox} values range between -1.65 and -2.48. The majority of the objects have values smaller than -2.0. They authors argue that the X-ray weakness of BAL quasars is due to neutral intrinsic absorption with column densities between about $(0.1–10) \times 10^{23}$ cm^{-2}. As more soft X-ray photons are expected for a simple neutral absorber, the authors argue that the absorption is more complex. Partial covering or ionized absorbers can account for this observational fact. However, LBQS 0102–2713 do not show such high values for the neutral absorber compared to BAL quasars. The foreground absorption is about 6×10^{20} cm^{-2}. This is at least a factor of about 20 lower compared to BAL quasars. LBQS 0102–2713 is an object which exhibits an unusual combination of UV brightness, X-ray weakness and no significant absorption by neutral matter along the line of sight. In addition, there are no significant indications that the object is intrinsically X-ray weak, in contrast to the argumentation for PHL 1811 by Leighly et al. (2007). This parameter combination is new and needs to be explained. With the present available X-ray data, we are limited in providing self-consistent models but would like to present these new results to the community.

7.2. LBQS 0102–2713 as a Supersoft Quasar

The object might exhibit the steepest photon index reported from a quasar so far. For a simple power-law fit with neutral absorption left free in the fit we get photon indices of $\Gamma = (5.8 \pm 1.3)$ *or* (6.0 ± 1.3) by using the *xselect* command line interface and the *EXSAS* software package, respectively. However, if the foreground N_H value is set to the Galactic value of 2×10^{20} cm^{-2} (Dickey & Lockman 1990) the photon index is about 3.5 (compared to the Γ–N_H contour plots shown in Figure 3). The photon index still remains steep compared to previous studies listed in Section 1. In addition, Puchnarewicz et al. (1995) applied a broken power-law fit to RE J2248-511 with a photon index of $4.13^{+5.85}_{-0.60}$ up to the break energy of 0.26 keV. The Galactic N_H value was fixed to 1.4×10^{20} cm^{-2}. For the object RE J1034+396 Puchnarewicz et al. (1995) obtain for their broken power-law fit a value of $\Gamma = 4.45^{+0.25}_{-0.32}$ up to a break energy of 0.41 keV. The N_H value was fixed to the Galactic value of 1.5×10^{20} cm^{-2}. We note that the low N_H values, although fixed to their Galactic values, result in similar steep photon indices as obtained for LBQS 0102–2713 with the N_H value fixed in the fit.

7.3. Open Problems

There are open problems which cannot be solved given the present set of multiwavelength data. First, we found that the UV emission is discontinuous to the X-ray emission, e.g., the UV photons which are expected to arise from the accretion disk appear not to be correlated with the X-ray photons. Second, if the steep soft photon index of (6.0 ± 1.3) will be confirmed by new X-ray observations this steepness needs to be explained. Based on the contour plots shown in Figure 3, the object might not be as extreme as one would expect from the simple power-law fits. Third, the UV luminosity density is about a factor of 10 more luminous compared to the mean of the most luminous SDSS quasars. However, as pointed out there is a large spread in the M_B magnitudes for quasars and the UV brightness might also show a large scatter compared to the mean value at a certain frequency. Finally, if the 2 keV X-ray weakness is confirmed by other observations, the combination of UV brightness, X-ray weakness and

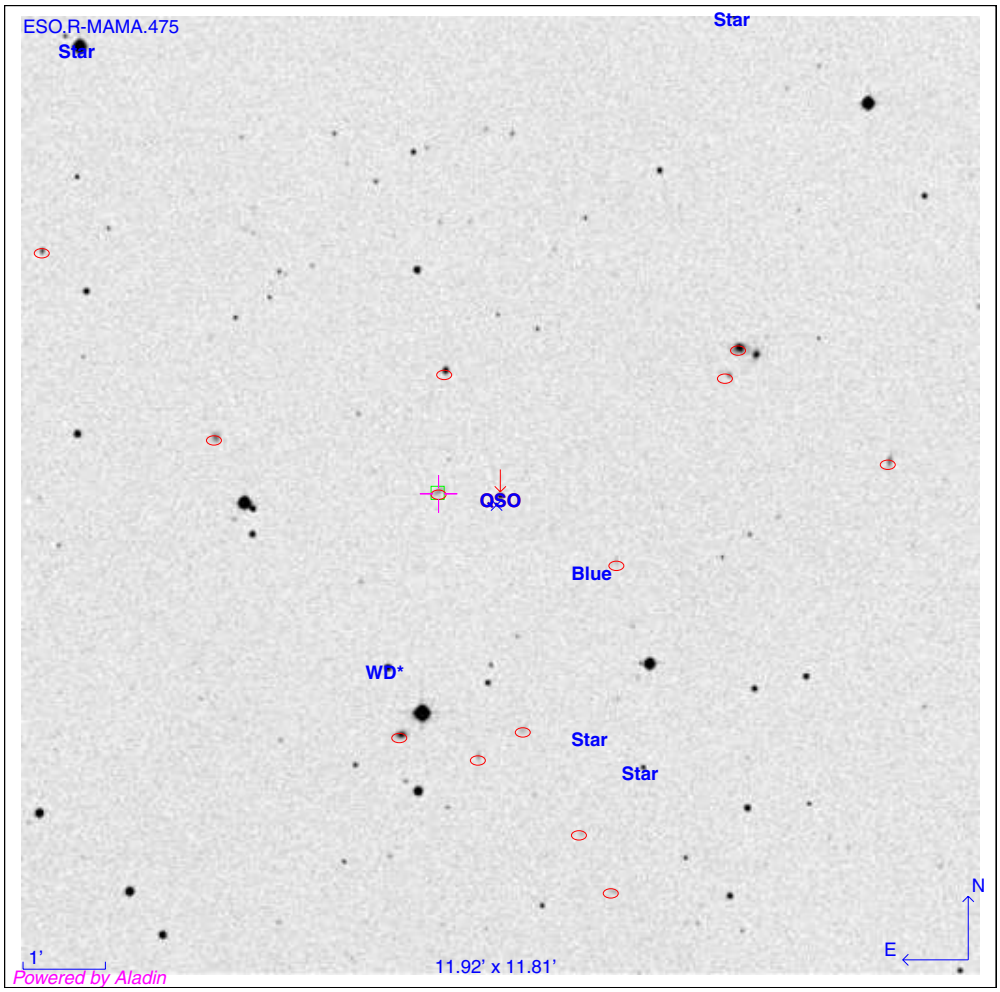

Figure 8. ESO R-MAMA.475 image with SIMBAD and NED detections overlaid. The SIMBAD objects are blue colored and the red circles indicate the NED detections. The box size is $10' \times 10'$. LBQS 0102–2713 is located in the center.
(A color version of this figure is available in the online journal.)

Table 3
SIMBAD Detection Within a 500 arcsec Radius Around LBQS 0102–2713

Identifier	Dist (arcsec)	Type	ICRS (2000) Coord.	Sp Type
HB89 0102–272	0.00	QSO	01 04 40.94 −26 57 07.5	···
1RXS J010441.1–265712	5.44	X	01 04 41.10 −26 57 12.5	···
PHL 7126	84.37	blu	01 04.60.00 −26 58 00.0	···
675	148.54	WD*	01 04 47.00 −26 59 12.0	···
GEN+6.20077018	184.71	*	01 04.60.00 −27 00 00.0	···
GSGP 1	220.57	*	01 04 33.30 −27 00 23.0	···
CGG* SGP 51	384.71	*	01 04 28.60 −26 51 20.0	G5
GSA 55	425.46	G	01 04 27.00 −27 03.50.0	···
CGG* SGP 68	444.42	*	01 05 03.80 −26 51 45.0	G5
RG 0102.6–2720	484.81	*	01 05.00.00 −27 04 00.0	···

the absence of significant absorption by neutral matter results into an unusual combination observational parameters which cannot be explained with the available set of multiwavelength data. Finally, what is the spectral complexity in the soft and hard X-ray band unresolvable for *ROSAT*? We know from observations with the present generation of X-ray telescopes that new spectral components can often be added to the fit and that the real spectrum might be more complex. We expect to see this in the soft band with higher signal-to-noise observations. In addition, observations above 2.4 keV are required to better constrain physical models for the unusual observational parameters detected in LBQS 0102–2713.

8. SECURITY CHECK

The probability that the X-rays arise from nearby sources is low. The total 1σ position error of the *ROSAT* detection is 7 arcsec including a 6 arcsec systematic error (see Voges et al.

Table 4
NED Detection Within a Radius of 500 arcsec Around the Source Position of LBQS 0102–2713

Object Name	R.A.	Decl.	Type	z	Dist (arcmin)
LBQS 0102–2713	01h04m40.9s	−26d57m07s	QSO	0.780000	0.0
2dFGRS S212Z160	01h04m44.3s	−26d57m05s	G	0.113844	0.8
APMUKS(BJ)B010210.33–271359.0	01h04m34.7s	−26d57m55s	G		1.6
2dFGRS S213Z276	01h04m44.0s	−26d55m38s	G	0.128000	1.6
APMUKS(BJ)B010215.35–271559.7	01h04m39.7s	−26d59m55s	G		2.8
2dFGRS S213Z278	01h04m28.9s	−26d55m40s	G	0.127000	3.0
2MASX J01044626-2659591	01h04m46.3s	−27d00m00s	G	0.156813	3.1
APMUKS(BJ)B010217.75–271619.8	01h04m42.1s	−27d00m16s	G		3.1
2MASX J01042726-2655252	01h04m28.2s	−26d55m20s	G	0.128500	3.4
2dFGRS S213Z275	01h04m56.4s	−26d56m26s	G	0.158043	3.5
APMUKS(BJ)B010212.20–271714.6	01h04m36.6s	−27d01m10s	G		4.2
2dFGRS S212Z166	01h04m20.1s	−26d56m42s	G	0.129330	4.7
APMUKS(BJ)B010210.57–271755.8	01h04m34.9s	−27d01m51s	G		4.9
APMUKS(BJ)B010241.39–271015.9	01h05m05.7s	−26d54m12s	G		6.3
APMUKS(BJ)B010215.35–271953.3	01h04m39.7s	−27d03m49s	G		6.7
2dFGRS S212Z165	01h04m28.9s	−26d50m54s	G	0.112910	6.8
2dFGRS S212Z164	01h04m32.8s	−26d50m11s	G	0.128985	7.2
APMUKS(BJ)B010245.29–270904.2	01h05m09.6s	−26d53m01s	G		7.6
APMUKS(BJ)B010251.36–271413.7	01h05m15.7s	−26d58m10s	G		7.8
MDS ua-01-09	01h04m35.0s	−27d04m54s	G	0.611600	7.9
APMUKS(BJ)B010224.51–270526.6	01h04m48.9s	−26d49m23s	G		8.0
APMUKS(BJ)B010252.42–271158.3	01h05m16.7s	−26d55m55s	G		8.1

(1999) and the link to the source catalog entries). The nearest SIMBAD source has a distance to the position of LBQS 0102–2713 of 84 arcsec resulting into a discrepancy of 12σ in the position offset. The same holds for the NED detections. The next source is at a distance of 0.8 arcmin resulting into a position error offset of about 7σ. In Figure 8, we show the optical image with the SIMBAD and NED detections overlayed. In Tables 3 and 4, we list objects within a distance of 500 arcsec to the position of LBQS 0102–2713.

The paper is based on observations obtained with the *ROSAT* PSPC satellite. We thank the anonymous referee for his/her extremely helpful comments to improve the scientific content and the structure of the paper. T.B. is grateful for intensive discussion with Ari Laor and Narum Arav on the UV–X-ray relations in quasars and especially on the object properties presented in this paper. T.B. acknowledges many comments from Niel Brandt on the UV and X-ray properties reported in this paper and on his intensive suggestions with respect to the comparison to BAL quasars. T.B. thanks Chris Done for providing her ionized absorber model and many suggestions to improve the paper. T.B. is also grateful to Gordon Richards for providing the super mongo script for the SED of radio-loud and radio-quiet quasars. T.B. would like to thank Michael Rosa for his information regarding the *HST* FOS flux calibration for LBQS 0102–2713 and Don Neill for his help to achieve precise information regarding the *GALEX* data. K.L. is grateful to the Secondary School Neu-Isenburg for their support to work together with T.B. at MPE Garching in analyzing the multiwavelength data presented in this paper. T.H. greatly acknowledges the collaboration with T.B. and W.G. in writing up this paper. The authors acknowledge Iskra Strateva, Frank Haberl, Marcella Brusa, and Konrad Dennerl for many helpful suggestions and information on the data presented in this paper. This research has made use of the NASA/IPAC Extragalactic Database (NED) which is operated by the Jet Propulsion Laboratory, California Institute of Technology, under contract with the National Aeronautics and Space Administration.

Facilities: *ROSAT*, *HST* FOS, *GALEX*.

REFERENCES

Boller, Th., Brandt, W., & Fink, H. 1996, A&A, 305, 53
Boller, Th., Brandt, W. N., Leighly, K. M., & Ward, M. J. (ed.) 2000, New Astron. Rev. 44, Proc. Workshop on Observational and Theoretical Progress in the Study of Narrow-Line Seyfert 1 Galaxies (Oxford: Elsevier)
Boller, Th., Fabian, A. C., Sunyvaev, R., Trümper, J., Vaughan, S., Ballantyne, D. R., & Brandt, W. N. 2002, MNRAS, 329, 1
Boller, Th., Tanaka, Y., Fabian, A. C., Brandt, W. N., Gallo, L., Anabuki, N., Haba, Y., & Vaughan, S. 2003, MNRAS, 343, 89
Brandt, W., Mathur, S., & Elvis, M. 1997, MNRAS, 285, 25
Brotherton, M. S., Arav, N., Becker, R. H., Tran, H. D., Gregg, M. D., White, R. L., Laurent-Muehleisen, S. A., & Hack, W. 2001, ApJ, 546, 134
Crummy, J., Fabian, A. C., Gallo, L., & Ross, R. R. 2006, MNRAS, 365, 1067
Dickey, J. M., & Lockman, F. J. 1990, ARA&A, 28, 215
Elvis, M., et al. 1994, ApJS, 95, 1
Fiore, F., Matt, G., Cappi, M., Elvis, M., Leighly, K. M., Nicastro, F., Piro, L., Siemiginowska, A., & Wilkes, B. J. 1998, MNRAS, 289, 103
Gallagher, S. C., Brandt, W. N., Chartas, G., Priddey, R., Garmire, G. P., & Sambruna, R. M. 2006, ApJ, 644, 709
Geminale, A., & Popowski, P. 2005, arXiv:astro-ph/0502540
George, I. M., Turner, T. J., Yaqoob, T., Netzer, H., Laor, A., Mushotzky, R. F., Nandra, K., & Takahashi, T. 2000, ApJ, 531, 52
Gibson, R. R., Brandt, W. N., & Schneider, D. P. 2008, ApJ, 685, 773
Green, P. J., et al. 2008, ApJ, 690, 644
Grupe, D., Beuermann, K., Mannheim, K., Thomas, H.-C., Fink, H., & de Martino, D. 1995, A&A, 300, 21
Hogg, D. W. 2000, arXiv:astro-ph/9905116v4
Hook, I. M., McMahon, R. G., Boyle, B. J., & Irwin, M. J. 1994, MNRAS, 286, 305
Leighly, K. M., Halpern, J. P., Jenkins, E. B., & Casebeer, D. 2007, ApJS, 173, 1
Miniutti, G., Fabian, A. C., Brandt, W. N., Gallo, L. C., & Boller, Th. 2009, arXiv:0904.3194v1
Morris, S. L., et al. 1991, AJ, 102, 1627
Morrissey, P., et al. 2007, ApJS, 173, 682
Nandy, K., Thompson, G. I., Jamar, C., Monols, A., & Wilson, R. 1975, A&A, 44, 195
Osterbrock, D. E., & Pogge, R. W. 1985, ApJ, 297, 166

Pounds, K. A., Done, C., & Osborne, J. P. 1995, MNRAS, 277, 5
Puchnarewicz, E. M., Branduardi-Raymont, G., Mason, K. O., & Sekiguchi, K. 1995, MNRAS, 276, 1281
Puchnarewicz, E. M., Mason, K. O., Siemiginowska, A., Cagnoni, I., Comastri, A., Fiore, F., & Fruscione, A. 2001, ApJ, 550, 874
Puchnarewicz, E. M., et al. 1992, MNRAS, 256, 589
Richards, G., et al. 2006, ApJS, 166, 470
Richstone, D. O., & Schmidt, M. 1980, ApJ, 235, 361
Schurch, N., & Done, C. 2006, MNRAS, 371, 81
Strateva, I. V., Brandt, W. N., Schneider, D. P., Vanden Berk, D. G., & Vignali, C. 2005, AJ, 130, 387
Tanaka, Y., Boller, Th., & Gallo, L. 2005, in Proc. MPA/ESO/MPE/USM Joint Astronomy Conf., Growing Black Holes: Accretion in a Cosmological Context, ed. A. Merloni et al. (Berlin: Springer), 290
Trümper, J. E., & Hasinger, G. 2008, The Universe in X-Rays (Berlin: Springer)
Vanden Berk, D. E., et al. 2001, AJ, 122, 549
Vignali, C., Brandt, W. N., & Schneider, D. P. 2003, AJ, 125, 433
Voges, W., et al. 1999, A&A, 349, 289
Walter, R., & Fink, H. 1993, A&A, 274, 105
Weedman, D. W. 1986, Quasar Astronomy (Cambridge: Cambridge Univ. Press)
York, D. 1990, *HST* Proposal 6007, Comparison of Large Scale Structure in QSO Absorbers and Galaxies at the Galactic Poles (Chicago: Univ. Chicago Press)
Zheng, W., Kriss, G. A., Telfer, R. C., Grimes, J. P., & Davidsen, A. F. 1997, ApJ, 475, 469
Zimmermann, U., Becker, W., Belloni, T., Döbereiner, S., Izzo, C., Kahabka, P., & Schwentker, O. 1994, MPE Report, 257 EXSAS User's Guide (4th ed.; Garching: MPE)